Seven-coordinated iron(II) spin-crossover molecules: some learning from iron substitution in [FexMn1−x(L222N3O2)(CN)2]×H2O solid solutions

Hongfeng Wang, Cherif Baldé, Arnaud Grosjean, Cédric Desplanches, Philippe Guionneau, Guillaume Chastanet

Cite this: DOI: 10.1039/c0xx00000x

ARTICLE TYPE

Seven-coordinated iron(II) spin-crossover molecule: some learning from iron substitution in the $[Fe_xMn_{1-x}(L_{222}N_3O_2)(CN)_2]\cdot H_2O$ solid solutions

Hongfeng Wang[a], Chérif Baldé[b], Arnaud Grosjean[a], Cédric Desplanches[a,*], Philippe Guionneau[a] and Guillaume Chastanet[a,*]

DOI: 10.1039/b000000x

The purpose of this work is to study the influence of the substitution of Fe(II) by Mn(II) on the spin crossover behaviour of the $[Fe_xMn_{1-x}(L_{222}N_3O_2)(CN)_2]\cdot H_2O$ solid solutions where $L_{222}N_3O_2$ is a macrocyclic ligand = 2,13-dimethyl-6,9-dioxa-3,12,18-triazabicyclo[12.3.1]-octadeca-1(18),2,12,14,16-pentaene. The pure Fe(II) complex is known to present a change of the coordination number from 7 at high temperature to 6 at low temperature. The target of the solid solutions study was to investigate the effect of metal dilution on this coordination change. We have then measured the thermal spin crossover features as well as the metastable HS state lifetime generated by a rapid thermal quenching which was probed through the determination of the T(TIESST) value. A discussion of the spin-state as a function of temperature is given based on the phase diagram of this series and based on the investigation of the crystal structure of the $[Mn(L_{222}N_3O_2)(CN)_2]\cdot H_2O$ complex and its comparison with the published $[Fe(L_{222}N_3O_2)(CN)_2]\cdot H_2O$ master compound.

Introduction

In recent decades, the development of the electronics led to a tremendous growth of information technology to reduce the size of the components and to increase their efficiency. In this context, the design of molecular materials owing switchable properties at room temperature is a current challenge for synthetic chemists worldwide.[1-6] In the family of switchable compounds, spin-crossover (SCO) compounds are of particular interest. They are transition metal complexes whose electronic configuration can be switched between low-spin (LS) and high-spin (HS) states by different physical (temperature, pressure, light and electric field)[6,7] and chemical (pH, coordination number, vapor…)[8,9] stimuli. These switching abilities make SCO molecules and materials very attractive for optical switches or/and magneto-optical storage properties[3-8,10,11], especially in the case of iron(II)-based molecular complexes, the most studied compounds, since the spin crossover occurs between a diamagnetic LS state and a paramagnetic quintet HS state.

A promising property shown by some of the SCO systems is the excited spin state trapping phenomenon (either light-induced, i.e. LIESST effect or thermally-induced, i.e. TIESST effect).[12] In some SCO solids, a metastable high-spin state can be populated at low temperature either by irradiation into *d-d* or MLCT absorption band of the ground state, or by fast cooling. One of the major target of such excited state trapping concerns the increase of the lifetime of the trapped state. To do so, an early attempt to correlate the SCO temperature with the thermal relaxation temperature after LIESST was reported by Herber et al..[13] but it was really Hauser in 1991 who introduced the first quantitative guideline allowing some expectation on the lifetime of the photo-induced HS state.[14] Hauser has carefully investigated the dynamics of the photo-induced state in different diluted SCO compounds and demonstrated that its lifetime is inversely proportional to $T_{1/2}$. This relation became known as the inverse-energy-gap law.[14,15]

Later on, Létard et al. introduced the so-called T(LIESST) measurement, which aimed to estimate the limiting temperature above which the photoinduced HS metastable state was erased.[16] This approach has been applied up to now to more than eighty SCO materials and, by comparing the various materials, some chemical levers were evidenced.[17-23] In particular, the influence of the inner FeN_6 coordination sphere, more precisely the degree of coordination of the metal centre and the distortion of the coordination sphere, on the stabilization of the photoinduced HS state seems to be one of the key factors.[22-24] This finding lends support to the idea that the photomagnetic properties are somehow governed at the molecular scale and then linked to the inner metal coordination sphere.[23,25] In particular, it has been shown that ligand having high denticity in general, and macrocyclic ligand in particular, were favouring high T(LIESST) values. Following this ascertainment, we have decided to investigate the magnetic and photomagnetic properties of a large number of iron(II) complexes involving macrocyclic ligands.[26] It appeared that the high T(LIESST) or T(TIESST) values were associated with molecules exhibiting a change in their coordination sphere, between FeN_3C_2O and $FeN_3C_2O_2$ geometries. This can be viewed as a huge distortion of the coordination sphere along the SCO.

In the present work, we wanted to promote and study the interplay between the complex thermal spin crossover feature of one of these macrocyclic SCO complexes and the related T(TIESST) curve (Figure 1). To do so, we performed solid solutions of the nominal compound $[Fe(L_{222}N_3O_2)(CN)_2]\cdot H_2O$. Here, a solid solution means that the elastic interactions between the iron centres within the solid are more or less interrupted by the partial substitution of iron by a metal that does not undergo SCO. This approach has been successfully used to understand the thermal spin-crossover and the relaxation behavior[27] and also to generate the overlap between the T(LIESST) and the thermal

hysteresis curve[28]. Therefore, we report the influence of the introduction of Mn(II) ion on the modification of the thermal-SCO features as well as the metastability of the HS state generated by a thermal quenching. In addition, we present and discuss the X-ray diffraction crystal structures of the $[Mn(L_{222}N_3O_2)(CN)_2]\cdot H_2O$ complex as well as two metal diluted complexes, i.e. $[Fe_xMn_{1-x}(L_{222}N_3O_2)(CN)_2]\cdot H_2O$ with $x = 0.963 \pm 0.005$ and $x = 0.638 \pm 0.009$.

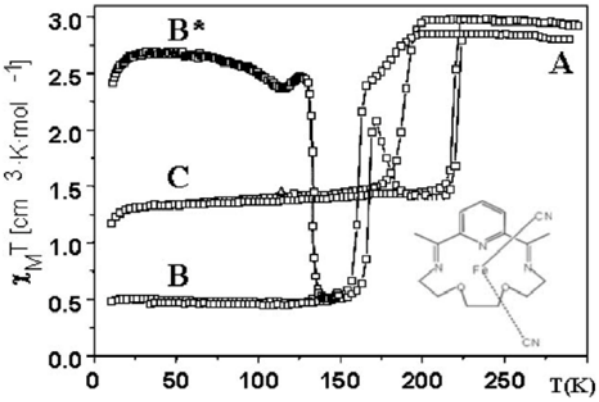

Fig. 1. Magnetic properties of $[Fe(L_{222}N_3O_2)(CN)_2]\cdot H_2O$ from previously reported SQUID measurements.[26b,26d]

Let us first recall that the different works already done have elucidated the atypical properties of $[Fe(L_{222}N_3O_2)(CN)_2]\cdot H_2O$. Figure 1 presents a summary of the various correlations between structure and magnetic properties (with χ_M being the molar magnetic susceptibility and T the temperature).[26b,26d] Briefly, the compound undergoes a thermal spin crossover at 155 K upon cooling but, depending on the experimental protocol, different phases and different levels of conversion can be achieved. Crystallographic studies clearly demonstrated that the HS to LS spin crossover occurs concomitantly with a modification of the metal environment from a 7 coordinence in the HS state to a 6 coordinence in the LS state.[26d] The resulting phase diagram appears quite complex (Figure 1). The phase **B** (LS-6 coordination) (T = 120 K, $P2_1/c$, a = 10.624(4) Å, b = 11.916(4) Å, c = 14.676(5) Å, β = 105.08(5)°, V = 1793.91(11) Å^3) appears from the slow cooling (of typically 2 hours, about 2 K min^{-1}) of the high spin state (HS-7 coordination), namely phase **A** (T = 300 K, C2/c, a = 17.326(5) Å, b = 12.054(5) Å, c = 10.125(5) Å, β = 116.27(1)°, V = 1896.2(13) Å^3). The phase **C** (T = 120 K, C2/c, a = 33.886(3) Å, b = 22.822(3) Å, c = 20.672(2) Å, β = 113.99(9)°, V = 14064.5(5) Å^3) attributed to the mixed HS/LS state may be reached if the cooling is much slower than 2 h. Being observed for the slowest cooling rate, phase C seems to be the ground state at low temperature. From the crystallography point of view, phase **C** corresponds to a stack of HS and LS complexes respectively hepta and hexa coordinated within the crystal-packing built from a unit-cell eight times larger than in phase **B**. Note that for phase **C**, the single-crystals quality systematically suffers from this transition which did not allow to get an accurate crystal-structure (R_{obs}= 0.19) preventing to describe in details intermolecular interactions for example but, due to the large modifications of intramolecular geometries in HS and LS, it was largely enough to distinguish between hepta- and hexa- entities.[29] Note that a crystal-structure refinement for phase C performed in the simple cell - thus with only one independent entity - (R_{obs} = 0.13) leads to Fe-ligands bond lengths intermediate of those expected in HS-hepta and LS-hexa.[29] The latter clearly demonstrated that the real structure of phase C is based on a mixture of HS-hepta and LS-hexa entities From phase **B** by irradiation a metastable HS state, Phase **B*** (T = 111 K, C2/c, a = 16.825(5) Å, b = 11.947(5) Å, c = 10.213(5) Å, β = 116.05(5)°, V = 1847.51(13) Å^3) can be obtained with a T(LIESST) of 135 K. Therefore, this compound appears as a very rare example of modification of degree of coordination triggered by SCO[26d,30]. Only another remarkable example from the same family of compound has been recently reported[31]. Regarding the properties' complexity of this system and the proximity of the T(LIESST) and the thermal SCO, $[Fe_xMn_{1-x}(L_{222}N_3O_2)(CN)_2]\cdot H_2O$ solid solutions are thus of high interest for the spin crossover community to promote unusual interplay between coordination change and metal dilution.

Experimental Section

Materials

The synthesis of the $[M^{II}(L_{222}N_3O_2)(CN)_2]\cdot H_2O$ complex (M = Fe^{II} or Mn^{II}) was performed by using the same protocol described by Nelson et al.[32] for the $[Fe(L_{222}N_3O_2)(CN)_2]\cdot H_2O$. The diluted compounds $[Fe_xMn_{1-x}]$ were synthesized according to the same procedure, replacing the metal salt by mixtures of iron(II) chloride and manganese(II) chloride in given ratios. The macrocyclic ligand $L_{222}N_3O_2$ is a Schiff base formed by condensation of a diketone and a diamine. Upon formation of the macrocyclic complex, M(II) ion is coordinated to the interior of $L_{222}N_3O_2$ ligand and two cyanide groups are then completing the coordination sphere of the ion M(II) in axial position. In detail, the synthesis of complexes was performed under anaerobic conditions (Schlenk line) and all solvents used were degassed. The reaction route is represented in Scheme 1 for Mn(II) analogue. The synthesis was carried out in 10 mL of methanol and 5 mL of water in which were dissolved 0.188 g (1.5 mmol) of manganese chloride, 0.25 g (1.5 mmol) of 2,6-diacetylpyridine, and 0.05 g of sodium dithionite. The 3,6-diamine dioxaoctane-1,8-diamine (0.23 mL, 1.5 mmol) was added dropwise. The mixture was kept at reflux under nitrogen gas for 16 h. A transparent orange solution was obtained. After filtration to remove impurities, 5 mL of aqueous solution containing an excess of sodium cyanide NaCN (1 g, 0.02 mol) was added, the solution turns dark orange. This solution was left in the fridge for two days, and then the brown crystals appeared in a cubic shape.

The elemental analysis of C, H, N was performed using a FlashEA^{TM} 1112 elemental analyzer. The values of the iron fractions (x) were calculated from the iron and manganese atomic percentages determined by quantitative analysis (ICP/OES Varian 720 ES), the sample being mineralized in hydrochloric acid prior to ICP analysis. The corresponding results are gathered in Table SI.1 in Electronic Supplementary Information (ESI). The experimental and calculated values are in good agreement (Fig. SI.1).

The composition of single crystals of mixed Fe/Mn compounds was obtained for two ratios, using a microprobe spectrometer CAMECA SX100. Ten crystals from the same synthetic batch of each ratio were measured, leading to the mean compositions $[Fe_xMn_{1-x}(L_{222}N_3O_2)(CN)_2]\cdot H_2O$ with $x = 0.963 \pm 0.005$ and $x = 0.638 \pm 0.009$. It indicates the strong homogeneity of the crystallization process and the resulting crystals.

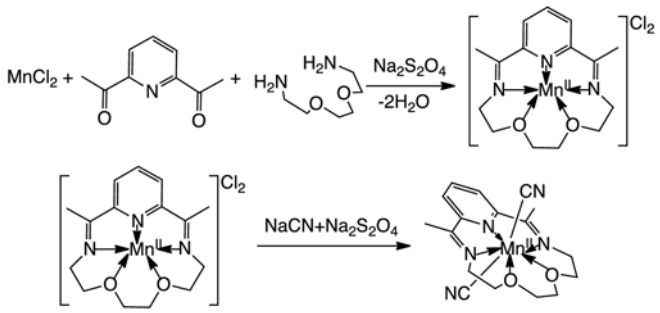

Scheme 1. Scheme of the synthesis of $[Mn(L_{222}N_3O_2)(CN)_2]\cdot H_2O$.

Physical Measurements

The thermal spin transitions of all the investigated compounds were followed in both cooling and warming modes by magnetic susceptibility measurements. $T_{1/2}\downarrow$ and $T_{1/2}\uparrow$ are usually defined as the temperatures for which there are 50% of LS and HS molecules in the cooling and warming modes, respectively. Magnetic susceptibilities were measured in the 10–300 K temperature range, under an applied magnetic field of 1 T, using a MPMS5 SQUID magnetometer (Quantum Device). The samples were precisely weighted and corrections (using Pascal constants) were applied to account for the compounds' and the sample holder's diamagnetic contributions. The procedure to record the T(TIESST) properties was as previously published.[16-18,20] The samples were rapidly quenched to 10 K by inserting the sample in less than 5 s from room temperature down to the cavity of the SQUID previously placed at 10 K. After thermal stabilization, the temperature was then slowly increased at 0.3 K min^{-1} and the extreme of the $\delta\chi_M T/\delta T$ *versus* T plots gave the T(TIESST) values.

Single crystal X-ray diffraction data for the structure determination of the three complexes were collected using a Bruker-Nonius diffractometer κ-CCD (λ = 0.7170 Å) at 300 K and 120 K to mimic the data published for the iron analogue.[26d] The crystal structures were determined and refined using SHELX-97 and SHELX-2013[33] within the WinGX environment.[34]. Cif files were deposited at CCDC under the numbers CCDC 1849970-1849974. All the crystal structures are of very good quality (table SI2-SI4). The powder X-Ray diffraction were performed on a PANalytical X'Pert Pro diffractometer.

Results and Discussion

Structural characterization.

The X-ray powder diffraction of $[Fe(L_{222}N_3O_2)(CN)_2]\cdot H_2O$ and diluted compounds $[Fe_xMn_{1-x}]$ have been recorded and all the compounds appeared isostructural (see Fig. SI.2). Crystals of the $[Mn(L_{222}N_3O_2)(CN)_2]\cdot H_2O$ complex as well as two metal diluted complexes, i.e. $[Fe_xMn_{1-x}(L_{222}N_3O_2)(CN)_2]\cdot H_2O$ with $x = 0.963 \pm 0.005$ and $x = 0.638 \pm 0.009$, suitable for Single-Crystal X-ray analysis were obtained by using the same protocol previously described for the neat iron(II) compound.[22]

Structural determination of $[Mn(L_{222}N_3O_2)(CN)_2]\cdot H_2O$ was firstly performed at 270 K. The $[Mn(L_{222}N_3O_2)(CN)_2]\cdot H_2O$ complex presents a hepta-coordinated state ($MnN_3C_2O_2$), in a monoclinic C2/c space group. The Mn(II) atom is in a pentagonal bipyramidal environment and is located on a twofold axis. The asymmetric unit contains only half of a complex. The bond lengths around manganese atom are : Mn1-N1 : 2.214(1) Å, Mn1-N2 : 2.2676(9) Å, Mn1-O1 : 2.308(1) Å and Mn1-C1 2.284(2) Å. The cell parameters at 270 K (a = 17.5613(3) Å, b = 12.0994(2) Å, c = 10.17850(10) Å, β = 116.5790(10)°, V = 1934.18(5) $Å^3$, Z = 4) are similar to the ones of the iron(II) analogue. At 120 K $[Mn(L_{222}N_3O_2)(CN)_2]\cdot H_2O$ stays in the monoclinic C2/c space group (a = 17.093(3) Å, b = 11.990(2) Å, c = 10.330(2) Å, β = 113.011(2)°, V = 1893.1(8) $Å^3$, Z = 4). The bond lengths around manganese atom are ranging between : 2.14 and 2.15 Å for Mn-N_{pyr}; 2.68 and 2.69 Å for Mn-N_{imine}; 2.31 and 2.32 Å for Mn-O; 2.72 and 2.84 Å for Mn-C (N_{pyr} being the nitrogen of the pyridine ring and N_{imine} the nitrogen of the imine functions). The three Mn(II) centers remain in hepta-coordinate state at 120 K.

At 270 K (Fig.2a) and 120 K (Fig.2b), the hydrogen bonding between the water molecule and the axial cyanide anions from infinite one dimensional chain, similarly to phase **A** of the iron analogue.

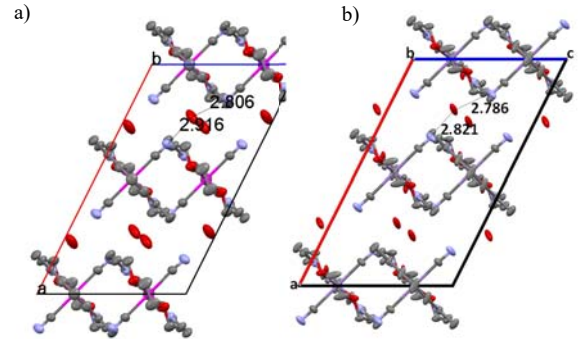

Fig. 2. Projection of the crystal packing of $[Mn(L_{222}N_3O_2)(CN)_2]\cdot H_2O$: a) 270 K; b) 120 K. Hydrogen atoms have been omitted for clarity.

For the diluted systems, in addition to the powder form, single crystals of $[Fe_xMn_{1-x}(L_{222}N_3O_2)(CN)_2]\cdot H_2O$ complexes (with x = 0.963 ± 0.005 and x = 0.638 ± 0.009) were also obtained by vapor diffusion method. Crystal determination of the two diluted compounds was performed at room temperature for both dilutions and at low temperature for the $[Fe_{0.638}Mn_{0.362}(L_{222}N_3O_2)(CN)_2]\cdot H_2O$ system (See crystal data in ESI). Nevertheless, despite our efforts it was impossible to solve the structure of $[Fe_{0.963}Mn_{0.037}(L_{222}N_3O_2)(CN)_2]\cdot H_2O$ complex at low temperature. These crystals are isomorphous at room temperature with pure $[Mn(L_{222}N_3O_2)(CN)_2]\cdot H_2O$ and $[Fe(L_{222}N_3O_2)(CN)_2]\cdot H_2O$. At low temperature, the $[Fe_{0.638}Mn_{0.362}(L_{222}N_3O_2)(CN)_2]\cdot H_2O$ compound keeps the same space group and similar cell parameters as at high temperature. Note that the attempts to distinguish Mn(II) atoms subsitute the Fe(II) atomic positions and the resulting Mn and Fe atomic positions was unsuccessful on the same site due to the vicinity of their atomic diffusion factor. This is the sign that iron and manganese are randomly distributed in the solid.

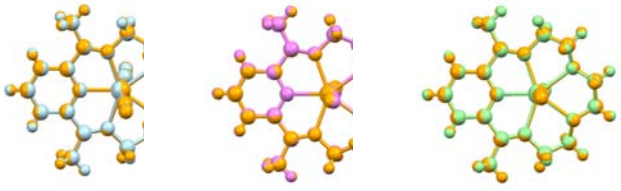

Fig. 3. Superposition of the $[Mn(L_{222}N_3O_2)(CN)_2]$ complex at room temperature (orange) with (a) $[Fe(L_{222}N_3O_2)(CN)_2]$ in HS (light blue), (b) $[Mn(L_{222}N_3O_2)(CN)_2]$ at low temperature (violet) and (c) with $[Fe_{0.638}Mn_{0.362}(L_{222}N_3O_2)(CN)_2]$ (light green).

The average Root-Mean-Square Deviation (RMSD) gives a basic comparison of the molecular shapes[24,35] through the superimposition of the different complexes studied here (Figure 3

and table SI.5). Learnings are: i) at room temperature, Mn and Fe complexes appear very similar, RMSD being indeed very small (0.058 Å) - the geometry taken for the manganese compound is the one for the pure compound $[Fe(L_{222}N_3O_2)(CN)_2]\cdot H_2O$ at 300 K (phase **A** of figure 1) -; ii) the structural transition that occurs at low temperature in the Mn complex crystal-packing also affects its molecular geometry, the average RMSD between RT and LT is weak (0.085 Å) but the maximum (0.267 Å) looks quite high indicating significant changes; iii) the average complex in Fe_xMn_{1-x} compounds is very close to the Fe one (RMSD from 0.012 to 0.021 Å); iv) when x decreases the average Fe_xMn_{1-x} complex moves towards the Mn one - incidentally, this means that the geometry of the Mn ion is the same in a Fe matrix, thus within the Fe_xMn_{1-x} crystal-packing, as in the Mn crystal-packing - and v) in Fe_xMn_{1-x} compounds, for x=0.64, the molecular shape is identical at high and low temperature - this means that all the Fe complexes are in HS whatever the temperature. The relatively high RMSD values obtained between $Fe_{0.64}Mn_{0.36}$ and Mn complexes at low temperature (0.095 Å) reveal that thermal-induced structural effects are also frozen in the Mn complexes within the Fe_xMn_{1-x} material.

All studied compounds are isostructural, having the same C2/c space group and similar cell parameters than phase **A** of pure Fe compound. The studied compounds retain the same structure when the temperature is decreased unlike the pure Fe compound that shows a modifications of space group at low temperature when Fe ions change of spin-state. It seems that since Mn complex remains seven coordinated whatever the temperature, when diluted in a surrounding of Mn complexes, the Fe complexes also remain in their high spin state, the HS to LS conversion of Fe being blocked by the high spin Mn complexes. To support this assumption, note that the favoring of the HS state of Fe by the introduction of Mn is also clearly observed by magnetic measurements (vide infra).

Magnetic characterization.

In this present work, we focus on the influence of Mn(II) dilution on the thermal SCO as well as on the metastability of the HS state generated by a rapid thermal quenching. The influence of the cooling and warming rate on SCO properties is also emphasized.

The magnetic behavior of the metal diluted $[Fe_xMn_{1-x}(L_{222}N_3O_2)(CN)_2]\cdot H_2O$ is recorded through the thermal dependence of the $\chi_M T$ product. For the two $[Fe(L_{222}N_3O_2)(CN)_2]\cdot H_2O$ and $[Mn(L_{222}N_3O_2)(CN)_2]\cdot H_2O$ complexes, the $\chi_M T$ values at room temperature were experimentally measured as 3.01 cm^3mol^{-1} K and 4.38 cm^3mol^{-1} K. For pure Mn(II) complex, $\chi_M T$ product remained constant down to 10 K, in agreement with the Mn(II) ion remaining high spin between room temperature and 10 K. the The $\chi_M T$ product of the diluted $[Fe_xMn_{1-x}]$ systems was found to increase with the metal dilution due to the paramagnetic contribution of the manganese(II) ion (d^5, S = 5/2). The $\chi_M T$ product is, in fact, the sum of the contributions of iron(II) and manganese(II) ions (Eq. (1)), and consequently the $\chi_M T$ relative to 1 mol of [Fe] entities is expressed by Eq. (2). The HS fraction (γ_{HS}) of iron(II) ions is finally directly proportional to $(\chi_M T)_{Fe}$ since the LS state of iron(II) is diamagnetic (Eq. (3)). The $T_{1/2}$ value was estimated as the temperature at which γ_{HS} takes the particular value $\gamma_{HS} = (1 - r_{HS})/2$, with r_{HS} the residual paramagnetic quantity at low temperature (i.e. 50 K).

$$\chi_M T = x(\chi_M T)_{Fe} + (1-x)(\chi_M T)_{Mn} \quad (1)$$

$$(\chi_M T)_{Fe} = \frac{\chi_M T - (1-x)(\chi_M T)_{Mn}}{x} \quad (2)$$

$$\gamma_{HS} = \frac{(\chi_M T)_{Fe}}{(\chi_M T)_{Fe}^{HT}} \quad (3)$$

It has been demonstrated for the $[Fe(L_{222}N_3O_2)(CN)_2]\cdot H_2O$ compound that the magnetic and photomagnetic properties originate within the thermal spin crossover history.[26b] Depending on the thermal pre-treatment of the complex, two different forms can be reached at low temperature, respectively the LS state and the LS/HS state. In fact, when the cooling rate was 3 K/min the LS form was effectively measured at low temperature while with a rate of 1 K/min only the LS/HS mixture state was found.[26b] Thus we decided, first, to study the influence of the cooling and warming rate on SCO properties of the diluted $[Fe_xMn_{1-x}]$ systems. To illustrate this effect, we investigate the influence of the rate of changing the temperature for two mixed complexes with $x = 0.966$ and $x = 0.949$. The temperature dependence of $(\chi_{MT})_{Fe}$ is presented in Fig.4 with temperature scan rates from 1 $Kmin^{-1}$ to 5 $Kmin^{-1}$.

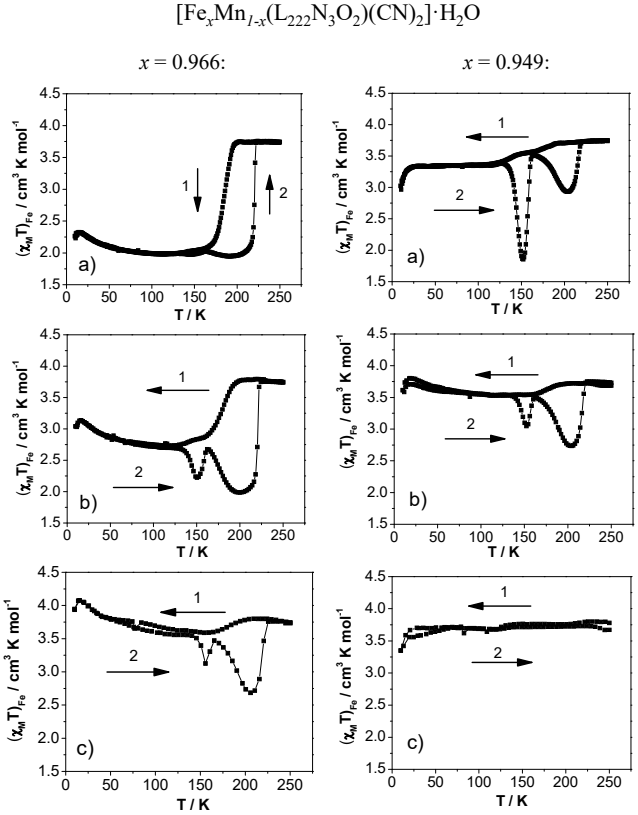

Fig.4. Temperature dependence of $(\chi_M T)_{Fe}$ for $[Fe_xMn_{1-x}(L_{222}N_3O_2)(CN)_2]\cdot H_2O$ with $x = 0.966$ (left) and x = 0.949 (right) at a) 1 $Kmin^{-1}$; b) 2 $Kmin^{-1}$ and c) 5 $Kmin^{-1}$. Solid lines are added in order to follow the SCO properties. The measurements were preformed first on cooling (1), then on warming (2).

For x = 0.966, with a rate of 1 $Kmin^{-1}$, the spin crossover is incomplete ($T_{1/2}\downarrow$ = 185 K, $T_{1/2}\uparrow$ = 220 K), with a hysteresis loop of 35 K. The $(\chi_M T)_{Fe}$ product at 150 K is equal to 1.98 $cm^3mol^{-1}K$ (γ_{HS} = 0.53). In regard to the pure $[Fe(L_{222}N_3O_2)(CN)_2]\cdot H_2O$ complex, this behavior can be attributed to the transition between HS state and the mixed HS/LS state. Only the width of the hysteresis is slightly reduced in regard to the iron complex (40 K).[26b] At a rate of 2 $Kmin^{-1}$, a gradual transition occurs in the vicinity of 200 - 160 K with $T_{1/2}\downarrow$ = 179 K with a very high residue at 110 K (γ_{HS} = 0.72). On the warming mode, the magnetic signal

displays a bump and recovers the initial HS $(\chi_M T)_{Fe}$ value at $T_{1/2}\uparrow$ = 220 K. In the case of 5 Kmin^{-1}, the magnetic signal slightly decreases on the cooling mode but remains almost in HS state even until 110 K (γ_{HS} = 0.98). On the warming mode, the magnetic behavior is similar to the rate of 1 Kmin^{-1} and 2 Kmin^{-1}, with the occurrence of a bump. To summarize, the $[Fe_xMn_{1-x}(L_{222}N_3O_2)(CN)_2]\cdot H_2O$ complex with x = 0.966 presents a strong influence of the temperature scan rate. With a rate of 1 Kmin^{-1}, the behavior is similar to the properties of the pure $[Fe(L_{222}N_3O_2)(CN)_2]\cdot H_2O$ in its second thermal cycle; i.e. a transition from HS state to HS/LS mixed state. With higher cooling rate, the HS state appears partially quenched. With a rate of 5 Kmin^{-1}, the spin change of iron compound can only be observed upon warming.

For x = 0.949, with the cooling mode of 1 Kmin^{-1}, the magnetic signal first decreases down to 3.40 cm^{3}mol^{-1}K (110 K, γ_{HS} = 0.91) and then remains stable. On the warming mode, the magnetic signal first decreases in the vicinity of 110 K to 150 K, reaching 1.85 cm^{3}mol^{-1}K at 151 K (γ_{HS} = 0.49), then increases. A second decrease can be observed at 160 K, reaching a minimum of 2.93 cm^{3}mol^{-1}K at 202 K (γ_{HS} = 0.78). Finally (χ_{MT})Fe value recovers the initial value of HS state. For 2 Kmin^{-1}, the magnetic behavior is very similar to results obtained with a cooling rate of 1 Kmin^{-1}. We observe the same bump on the warming mode with two minimum at 152 K with a value of 3.05 cm^{3}mol^{-1}K (γHS = 8.16) and at 202 K with a value of 2.73 cm^{3}mol^{-1}K (γHS = 0.73). For 5 Kmin^{-1}, the behavior is totally different. The magnetic signal remains stable during the cooling mode and the warming mode. Almost all the iron(II) ions remain kinetically blocked into the HS state.

The insertion of Mn(II) ions into the lattice strongly affects the SCO properties (Figure 4 compare to Figure 1). If we consider for instance a constant cooling rate of 1 Kmin^{-1}, the metal diluted complex (x = 0.949) displayed a very high HS residual fraction (Fig.4a right), while for x = 1 (Fig.3) and x = 0.966 (Fig.4a left), a HS to HS/LS mixed state transition can be observed. This tendency is confirmed at a rate of 5 Kmin^{-1}, where Fe(II) remains HS at any temperature for x = 0.949. By increasing the percentage of the Mn(II) ions, the kinetics of the SCO phenomenon is slowed down while cooled down. Moreover, on warming those complexes display a decrease of $(\chi_M T)_{Fe}$ value in the vicinity of 150 K to 200 K, and the magnitude becomes more negligible with lower x value (high dilution).

Several remarks can be done: ***i)*** on the first cooling experiment for none of the metal diluted complexes, it was possible to record the fully HS to LS transition. It seems that the insertion of Mn(II) ions tends to block the spin conversion of Fe complex between seven coordinated HS state and six coordinated LS state ; ***ii)*** for most of the measurements, on warming, $(\chi_M T)_{Fe}$ vs.T curve displays two minima at almost the same temperatures. Only the proportion is changing as function of the metal dilution; ***iii)*** The insertion of Mn(II) metal ions seems to strongly affect the kinetic of the SCO process. When the metal dilution increases, it is necessary to decrease the cooling rate to observe the SCO phenomenon. In other words, the lower the temperature scan rate, the higher the possibility to reach the HS/LS mixed state. On the contrary, increasing the temperature scan rate favors the inhibition of the SCO. These observations are somewhat in agreement with the previous remarks made in metal dilution studies.[26,36-39] In particular, when we reach the peculiar situation where the high temperature stable HS phase overlaps with the low temperature metastable HS state.[26,37c] It was demonstrated that the overlap between the two regimes favors the freezing of the SCO. More precisely, it has been suggested that HS state of Fe(II) is favoured by Mn(II) dilution due to the large ionic radius of the last (ionic radius are 83 pm for Mn(II) HS, 78 pm for Fe(II) HS and 63 pm for Fe(II) LS). To check the occurrence of such overlap, we investigated the quenching effect in the two metal diluted systems discussed before (x = 0.966 and x = 0.949). The simplest way to do so was to perform thermal trapping of the HS state.

For x = 0.966 two quenching experiments were performed. On the first experiment the magnetic signal was recorded immediately after trapping at 10 K with a warming rate of 1 Kmin^{-1} (Fig. 5a). The complex is then in the metastable HS* state up to 120 K and then in a few kelvins the $(\chi_M T)_{Fe}$ product drops drastically (position 2, Fig. 5a) to reach a minimum $(\chi_M T)_{Fe}$ value at 148 K (0.59 cm^{3}mol^{-1}K). This $(\chi_M T)_{Fe}$ product remains stable when temperature was cooled back to 10 K (position 3). On the contrary, when the temperature overpasses 150 K, the magnetic signal increases to reach a maximum at 163 K (3.44 cm^{3}mol^{-1}K, position 4) then decreases down to 2.00 cm^{3}mol^{-1}K at 205 K. A subsequent 1 hour kinetic experiment at 205 K did not further decrease the χ_MT value (position 5). The value remains even stable when temperature was further varied in the vicinity of 205 K – 10 K (position 6). From 205 K to 230 K the magnetic signal keeps increasing with a $T_{1/2}\uparrow$ = 220 K (position 7).

The second set of experiment performed on x = 0.966 (Fig. 5b) consists of a fast cooling of the sample at 10 K, in its 100% metastable HS* state, and to record the kinetic at 148 K during 4 hours. During the first hour, the $(\chi_M T)_{Fe}$ product strongly decreases to reach a value of 0.38 cm^{3}mol^{-1}K and then remains almost stable in the next 3 hours. Subsequent experiment by cooling temperature down to 10 K illustrated that this value is stable. From 148 K to 250 K the magnetic behavior seems to be similar with the first trapping experiment in Fig. 5a i.e. the formation of a maximum (position 4) and a minimum (position 5) before coming back to room temperature (HS state).

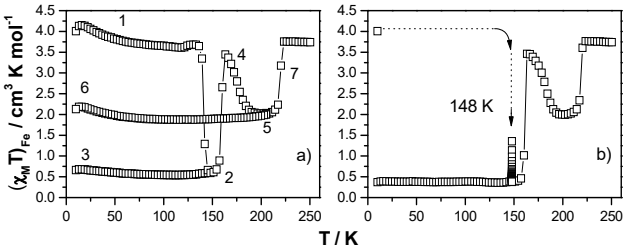

Fig. 5. Temperature dependence of $(\chi_M T)_{Fe}$ for $[Fe_xMn_{1-x}(L_{222}N_3O_2)(CN)_2]\cdot H_2O$ with x = 0.966 after fast cooling measurement: a) measurement started from 10 K. The numbering has been added to follow sequence of the measurement; b) kinetic at 148 K. Solid lines and dashed lines are added in order to follow the SCO behavior.

Concerning the complex $[Fe_xMn_{1-x}(L_{222}N_3O_2)(CN)_2]\cdot H_2O$ with x = 0.949 (Fig. 6), fast cooling experiments followed by heating at a warming rate of 1 Kmin^{-1} were also performed. The first set of measurement corresponds to a quenching from 10 K (Fig. 6a), and the second to study the relaxations at some selected temperature after trapping (Fig. 6b). From Fig.6a, it appears that under quenching at 10 K, the metastable HS* state is populated. Then, the $(\chi_M T)_{Fe}$ value only slightly decreases from 3.77 cm^{3}mol^{-1}K at 140 K to 2.90 cm^{3}mol^{-1}K at 154 K, suggesting a partial SCO of about 23%. After that, the magnetic signal increases immediately to reach a $(\chi_M T)_{Fe}$ value of 3.75 cm^{3}mol^{-1}K at 163 K. A very small decrease can be observed at around 160 K up to 202 K. Finally, the signal recovers its initial value. The Fig. 6b reports the results of the kinetics performed at 148 K and 190 K after fast cooling at 10 K (these kinetics are plotted as a function of time in figure SI6). It reveals that the LS state and the mixed HS/LS state

are totally masked and can be in fact reached by performing some relaxation at selected temperature.

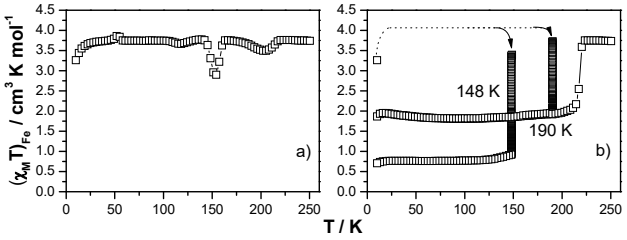

Fig. 6. Temperature dependence of $(\chi_M T)_{Fe}$ for $[Fe_xMn_{1-x}(L_{222}N_3O_2)(CN)_2]\cdot H_2O$ with x = 0.949 after fast cooling measurement with a rate of 1 $Kmin^{-1}$: a) measurement started from 10 K; b) kinetics at 148 K and 190 K. Solid lines and dashed lines are added in order to follow the SCO properties.

From these series of results, it is obvious that kinetic effects control the access of the LS and HS/LS state on the metal diluted systems. All that confirms that the transition behavior of the diluted series $[Fe_xMn_{1-x}(L_{222}N_3O_2)(CN)_2]\cdot H_2O$ with x = 0.966 and x = 0.949 is highly dependent on the temperature scan rate, something which was already true for the pure Fe compound (x = 1).

To complete this analysis, we have performed the thermal trapping of the HS state and recorded the T(TIESST) curve to extract the T(TIESST) value, the temperature above which the Thermally-Induced Excited Spin-State is erased.[16-18] T(TIESST) measurements have been done at 0.3 Kmn^{-1} for a selection of metal diluted complex with x = 1, 0.949, 0.930, 0.912, 0.892 and 0.853. Temperature dependence of $(\chi_M T)_{Fe}$ is presented in Fig. 7 and Table 1 collects the characteristic values. From the curves in Fig. 7, it can be seen that whatever the metal dilution, a first HS state (i.e HS_1) is obtained at 10 K, which corresponds to the metastable HS* state obtained by fast cooling. On warming from 10 K, a decrease of the magnetic signal is obtained in the vicinity of 130 K to 150 K. For convenience, we propose to name this state LS_1. The increase of Mn(II) percentage appears to rise the residual HS fraction as illustrated by the $(\chi_M T)_{Fe}$ value of LS_1. When the temperature is further increased up to 170 K, a new increase of the magnetic signal happens. We named the maximum HS_2. After that, the magnetic signal decreases to reach a minimum at around 205 K. In regard to $[Fe(L_{222}N_3O_2)(CN)_2]\cdot H_2O$ we propose to name this state LS_2/HS_3. Similarly to what has been observed for the LS_1 state, the minimum $(\chi_M T)_{Fe}$ of LS_2/HS_3 also increases significantly with an increase of Mn(II) percentage. Finally at around 220 K, the $(\chi_M T)_{Fe}$ value increases to recover its initial HS_4 value. Several comments can be made: ***i)*** with metal dilution, the evolution of $(\chi_M T)_{Fe}$ is less abrupt due to a decrease of the cooperativity of the system already observed for other systems[26,37c] ***ii)*** compared with Fe(II), for all the metal diluted complexes, HS_1 and HS_4 correspond to the Phase **B*** and Phase **A** respectively (Fig. 1). Attention has to be paid on the complex $[Fe_xMn_{1-x}(L_{222}N_3O_2)(CN)_2]\cdot H_2O$ with x = 0.853, which remains HS from 10 K to 250 K. In this case HS_1 and HS_4 can not be distinguished; ***iii)*** The LS_1 of the metal diluted complexes is associated with Phase **B** of pure Fe(II). We noticed an important increase of the $\chi_M T$ product of the LS_1 with the metal dilution. This can be understood by the previous works performed on dilution series,[26,37c] where complexes with Mn(II) metal dilution favor the HS state; ***iv)*** the LS_2/HS_3 in metal diluted system is associated with the Phase **C** of the pure iron complex (Fig. 1). Similarly with LS_1, the LS_2/HS_3 is under the strong influence of dilution effect.

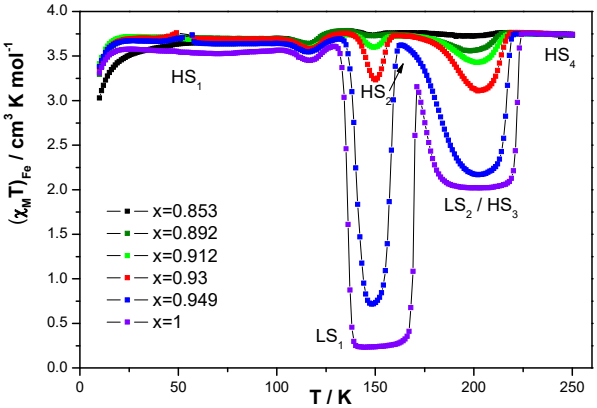

Fig. 7. Temperature dependence of $(\chi_M T)_{Fe}$ for $[Fe_xMn_{1-x}(L_{222}N_3O_2)(CN)_2]\cdot H_2O$ of T(TIESST) experiment with x = 1 (in violet ■), 0.949 (in blue ■), 0.93 (in red ■), 0.912 (in green ■), 0.892 (in olive ■) and 0.853 (in black ■).

Upon the TIESST experiments with a warming rate of 0.3 $Kmin^{-1}$, five characteristic temperatures for different Mn(II) percentage can be obtained. With an increase of temperature, those important temperatures appear in the following order (Fig. 8a): T(TIESST); T1: temperature at which 50 % of LS_1 has transited to HS_2; T2: temperature at which $(\chi_M T)_{Fe}$ is maximum, corresponding to HS_2; T3, temperature at which 50 % of HS_2 has transited to LS_2/HS_3 where obtains 50 % transition of LS_2/HS_3; and $T_{1/2}\uparrow$. The values of those temperatures are listed in Table 1. From x = 1 to x = 0.912, the five defined temperatures can be determined. For x = 0.853, none of the five temperatures are obtained. With this series of characteristic temperatures, we built the phase diagram presented on Fig. 8b.

Interestingly, the various characteristic temperatures indeed can be well fitted with a linear relation as a function of Mn(II) percentage. T(TIESST) and T1 define the region where LS_1 can be obtained. T3 and $T_{1/2}\uparrow$ give the region where the LS_2/HS_3 is formed. The linear fit of T(TIESST) and T1 meet at round 10.2 % Mn(II). In other words, above this percentage, the LS_1 could not be

Table1. Characteristic values obtained for the mixed $[Fe_xMn_{1-x}(L_{222}N_3O_2)(CN)_2]\cdot H_2O$ system (with x = 1, 0.949, 0.930, 0.912, 0.892 and 0.853).

SCO Systems	*T(TIESST) / K*	*T1 / K*	*T2 / K*	*T3 / K*	$T_{1/2}\uparrow$ / K	$(\chi_M T)_{Fe}$ at 148 K (LS_1)	$(\chi_M T)_{Fe}$ at 202 K (LS_2/HS_3)
x = 1	136	170	171	175	222	0.23	2.02
x = 0.949	140	158	163	182	217	0.71	2.16
x = 0.93	146	154	160	191	214	3.24	3.10
x = 0.912	145	153	157	191	212	3.59	3.42
x = 0.892	-	-	-	-	211	3.72	3.57
x = 0.853	-	-	-	-	-	3.72	3.72

obtained. This is in perfect agreement with experimental result of

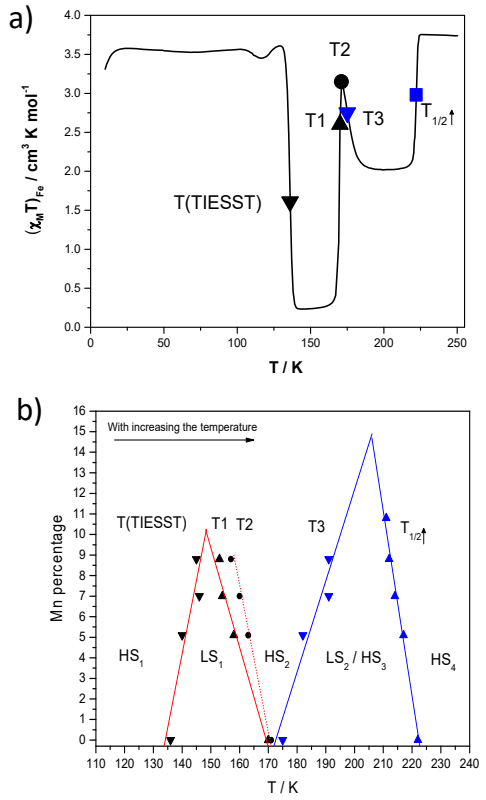

Fig. 8. a) Illustration of the five defined temperatures on a T(TIESST) curve. b) Phase diagram built from the characteristic temperatures for different Mn(II) percentage. ▼ T(TIESST); ▲ Temperature 1, ● Temperature 2; ▼ Temperature 3, and ▲ $T_{1/2}$↑. Solid and dotted lines in red and blue are the linear fit of the corresponding temperatures.

the complex with x = 0.892 (11%), where the LS_1 can not be reached during the TIESST measurement (Fig. 7). For LS_2/HS_3, the meeting point is predicted at 14.8 % of Mn(II). However at x = 0.892 (11%), the experiment results already show that the LS_2/HS_3 is barely observed. Finally, $T_{1/2}$↑ exhibits a decrease upon substitution of iron ions by manganese, as expected for such metal dilution. Indeed, metal dilution is known to exert an internal pressure that depends on the size of the host ion. A doping metal ion, having no spin crossover, corresponds to a unit-cell volume that differs from the one imposed by the iron ion. In the solid-solution, the bigger the doping ion, the larger the unit-cell and the larger is the volume available for the iron-ion within the crystal packing. Consequently, large unit-cells favor the state of larger volume of the iron(II), therefore the HS state. Accordingly, the temperatures $T_{1/2}$ are shifted to low temperatures when large metal ions are used to dope the SCO material; HS residue being also favored.[28, 37-39] Since manganese(II) ion has a larger ionic radius than the HS iron(II), a decrease of $T_{1/2}$ is expected.

Conclusions

In the present work, we have investigated the crystal structure of $[Mn(L_{222}N_3O_2)(CN)_2]\cdot H_2O$ and metal diluted $[Fe_xMn_{1-x}(L_{222}N_3O_2)(CN)_2]\cdot H_2O$ series. It was evidenced that the manganese centers were seven coordinated and the metal diluted series was isomorphous with the Mn(II) and Fe(II) analogues at room temperature. Contrary to the pure Fe compound, the compounds containing Mn do not show any phase transition upon cooling. From magnetic studies, strong kinetics effects were found in the powder samples of $[Fe_xMn_{1-x}(L_{222}N_3O_2)(CN)_2]\cdot H_2O$ series, which resulted in HS residual at low temperature depending on cooling rate. Upon warming, partial SCO from the HS state to the HS/LS mixed state occurred on several metal diluted samples, which was under strong influence of the cooling/warming rate, indicating interest in the investigation of TIESST properties of the metal diluted series. It has been observed that when $x \leq 0.892$, the samples remain almost in HS state during the whole TIESST measurement while the phase diagram appears more complicated for higher x values. Five temperatures have been defined to describe this phase diagram. As a result, clearly, playing on the dilution rate allows to control the degree of conversion and the temperature required to get the different phases.

As conclusion, we have observed that the SCO properties of the metal diluted complex are strongly influenced by the kinetic effect. In consequence, the transition between HS and LS_2/HS_3 states can be hidden if we consider the samples with $x \leq 0.892$. For this reason, we have decided to investigate in more detail the hidden transition, i.e. to probe by thermal relaxation and/or light irradiation to study whether the predicted HS to LS_2/HS_3 transition may appear. The work is currently in progress.

Conflicts of interest

There are no conflicts of interest to declare

Acknowledgements

We thank the Department of Cooperation and Cultural Action Embassy of France to Dakar-Sénégal, the University of Ziguinchor and its Department of Cooperation and Research, the Ministry of Higher Education and Research of Sénégal (Program FIRST) and CAMPUS France. This work was also supported by the University of Bordeaux, the CNRS, the Region Nouvelle Aquitaine and by the LabEx AMADEus (ANR-10-LABX-42) within IdEx Bordeaux (ANR-10-IDEX-03-02), i.e. the Investissements d'Avenir programme of the French government managed by the Agence Nationale de la Recherche. The ANR is also warmly acknowledge (ANR femtomat n° 13-BS04-002). The UMS PLACAMAT is acknowledged for the microprobe measurements.

Notes and references

[a]CNRS, Univ. Bordeaux, ICMCB, UMR 5026, F-33600 Pessac, France. Fax: (+33) 540002649. Tel (+33) 540002678. Email: guillaume.chastanet@icmcb.cnrs.fr , cedric.desplanches@icmcb.cnrs.fr
[b]Laboratoire de Chimie et Physique des Matériaux (LCPM) Université de Ziguinchor Bp: 523 Ziguinchor- Sénégal. Fax: (+221) 339916809. Tel (+221) 339916809. Email: cbalde@univ-zig.sn

1 a) J. M. Lehn, *Science*., 2002, 295, 2400; b) M. Ruben, U. Ziener, J. M. Lehn, V.Ksenofontov, P. Gütlich, G. B. M. Vaughan, *Chem. Eur. J*., 2005, 11, 94; c) M. Fujita, D. Oguro, M. Miyazawa, H. Oka, K. Yamaguchi, K. Ogura, *Nature*., 1995, 378, 469; d) O. M. Yaghi, M. O'Keeffe, N. W. Ockwig, H. K. Chae, M. Eddaoudi, J. Kim, *Nature*., 2003, 423, 705.
2 E. Breuning, M. Ruben, J. M. Lehn, F. Renz, Y. Garcia, V. Ksenofontov, P. Gütlich, E. Wegelius, K. Rissanen, *Angew. Chem*., 2000, 112, 2563; *Angew. Chem. Int. Ed*., 2000, 39, 2504.
3 Spin Crossover in Transition Metal Compounds I–III. In Topics in Current Chemistry; P. Gütlich. H-A. Goodwin., *Eds.; Springer-Verlag*: Berlin, Germany, 2004; Vols. 233–235.
4 O. Kahn, C. J. Martinez, *Science*., 1998, 279, 44.
5 A. Bousseksou, G. Molnar, L. Salmon, W. Nicolazzi, *Chem. Soc.Rev*., 2011, 40, 3313.
6 *a) Spin-Crossover Materials, Properties and Applications* (*Ed*.: M. A. Halcrow), John Wiley & Sons, *Ltd*., 2013; b) H. Banerjee, S. Chakraborty, T. Saha-Dasgupta, *Inorganics*, 2017, 5, 47; c) A.

Sugahara, H. Kamebuchi, A. Okazawa, M. Enomoto, N. Kojima, Inorganics, 2017, 5, 50
7 P. Gütlich, A. B. Gaspar, Y. Garcia, *Beilstein J. Org. Chem*., 2013, 9, 342.
8 a) M. M. Khusniyarov, *Chem. Eur. J*., 2016, 22, 15178; b) Z.-P. Ni, J.-L. Liu, N. Hogue, W. Liu, J.-Y. Li, Y.-C. Chen, M.-L. Tong, *Coord. Chem. Rev.*, 2017, 335, 28
9 J. Hasserodt, J. L. Kolanowski, F. Touti, *Angew. Chem. Int. Ed*., 2014, 53, 60; *Angew. Chem*., 2014, 126, 60.
10 K.S. Kumar, M. Ruben, *Coord. Chem. Rev*., 2017, 346, 176.
11 J.-F. Létard, P. Guionneau, L. Goux-Capes, *Top. Curr. Chem*., 2004, 235, 221.
12 a) S. Decurtins, P. Gütlich, C.P Kohler, H. Spiering, A. Hauser, *Chem. Phys. Lett.,* 1984, 105, 1 ; b) S. Decurtins, P. Gütlich, K.M Hasselbach, A. Hauser, H. Spiering, *Inorg. Chem*., 1985, 24, 2174; c) A. Hauser, *Chem. Phys. Lett*., 1986, 124, 543; d) A. Hauser, *Top. Curr. Chem*,, 2004, 234, 155.
13 a) R. Herber, L.M. Casson, *Inorg. Chem*., 1986, 25, 847; b) R. Herber, *Inorg. Chem*., 1987, 26, 173.
14 A. Hauser, *Coord. Chem. Rev*., 1991, 11, 275.
15 A. Hauser, C. Enaschescu, M. L. Daku, A. Vargas, N. Amstutz, *Coord. Chem. Rev.*, 2006, 250, 1642.
16 a) J.-F. Létard, P. Guionneau, L. Rabardel, J.A.K. Howard, A.E. Goeta, D. Chasseau, O. Kahn, *Inorg. Chem*., 1998, 37, 4432; b) M. Marchivie, P. Guionneau, J. F. Létard, D. Chasseau, J. A. K. Howard, *J. Phys. Chem. Solids.,* 2004, 65, 17.
17 J.-F. Létard, L. Capes, G. Chastanet, N. Moliner, S. Létard, J.-A. Real, O. Kahn, *Chem. Phys. Lett*., 1999, 313, 115.
18 S. Marcén, L. Lecren, H.A. Goodwin, J.-F. Létard, *Chem. Phys. Lett*., 2002, 358, 87.
19 a) S. Hayami, Z.-Z. Gu, Y. Einaga, Y. Kobayashi, Y. Ishikawa, Y. Yamada, A. Fujishima, O. Sato, *Inorg. Chem*., 2001, 40, 3240; b) J. S. Costa, P. Guionneau, J.-F. Létard, *J. Phys.: Conference Ser*., 2005, 21, 67.
20 a) N. Shimamoto, S.-S. Ohkoshi, O. Sato, K. Hashimoto, *Inorg. Chem*., 2002, 41, 678; b) R. Lebris, C. Mathonière, J.-F. Létard, *Chem. Phys. Lett*., 2006, 426, 380.
21 D. Li, R. Clérac, O. Roubeau, E. Harte, C. Mathonière, R. Le Bris, S. M. Holmes, *J. Am. Chem. Soc*., 2008, 130, 252.
22 J.-F. Létard, P. Guionneau, O. Nguyen, J.S. Costa, S. Marcén, G. Chastanet, M. Marchivie, L. Goux-Capes, *Chem. Eur. J*., 2005 11, 4582.
23 a) J. F. Létard, *J. Mater. Chem*. 2006, 16, 2550; b) J.-F. Létard, G. Chastanet, O. Nguyen, S. Marcén, M. Marchivie, P. Guionneau, D. Chasseau, P. Gütlich in "Molecular Magnets Recent Highlights", Eds W. Linert & M. Verdaguer, Springer Wien N.-Y. 2003, 49; c) J.-F. Létard, G. Chastanet, P. Guionneau, C. Desplanches, in Spin Crossover Materials: Properties and Applications, Ed. Malcom A. Halcrow, 2013, John Wilfreysey & sons, 475.
24 P. Guionneau, *Dalton Trans*., 2014, 43, 382.
25 S. Bonhommeau, N. Brefuel, V.K. Palfi, G. Molnar, A. Zwick, L. Salmon, J.-P. Tuchagues, J.S. Costa, J.-F. Létard, H. Paulsen, A. Bousseksou, *Phys. Chem. Chem. Phys*., 2005, 7, 2909.
26 a) P. Guionneau, J-S. Costa, J.-F. Létard, *Acta Cryst*., 2004, C60, m587; b) J-S. Costa, P. Guionneau and J-F. Létard, *Journal of Physics: Conf. Series*., 2005, 21, 67; c) J-S. Costa, C. Baldé, C. Carbonera, D. Denux, A. Wattiaux, C. Desplanches, J-P. Ader, P. Gütlich and J-F Létard, *Inorg. Chem*., 2007, 46, 4114; d) P. Guionneau, F. Le Gac, A. Kaiba, J-S. Costa, D. Chasseau and J-F. Létard, *Chem. Commun*., 2007, 3723-3725; e) R. Ababei, C. Pichon, O. Roubeau, Y-G Li, N. Bréfuel, L. Buisson, P. Guionneau, C. Mathonière and R. Clérac, *J. Am. Chem. Soc*., 2013, 135, 14840; f) H. Wang, C. Sinito, A. Kaiba, J-S. Costa, C. Desplanches, P. Dagault, P. Guionneau, J-F Létard, P. Negrier and D. Mondieig, *Eur. J. Inorg. Chem*., 2014, 4927–4933; g) H. Wang, A. Grosjean, C. Sinito, A. Kaiba,ab C. Baldé, C. Desplanches, J-F. Létard and P. Guionneau*, CrystEngComm*, 2015, 17, 4075.
27 (a) A. Hauser, *Coord. Chem. Rev*., 1991, 111, 275; (b) J. Jeftic and A. Hauser, *J. Phys. Chem. B.*, 1997, 101, 10262; (c) H. Romstedt, A. Hauser and H. Spiering, *J. Phys. Chem. Solids*., 1998, 59, 265; (d) A. Vef, U. Manthe, P. G ütlich and A. Hauser, *J. Chem. Phys*., 1994, 101, 9326; e) M.S. Sylla, C. Balde, N. Daro, C. Desplanches, M. Marchivie, G. Chastanet, *Eur. J. Inorg. Chem*. 2018, 297.
28 a) N. Paradis, G. Chastanet, J.-F. Létard, *Eur. J. Inorg. Chem.,* 2012, 3618 ; b) N. Paradis, G. Chastanet, F. Varret, J.-F. Létard, *Eur. J. Inorg. Chem*., 2013, 968 ; c) N. Paradis, G. Chastanet, T. Palamarciuc, P. Rosa, F. Varret, K. Boukheddaden, J.-F. Létard, *J. Phys. Chem. C.*, 2015, 119, 20039.
29 F. Le Gac, PhD, Univ. Bordeaux France, 2008
30 (a) R. T. Acha and M. Pilkington, *Cryst. Eng. Comm*, 2015, 17, 8897 and also Coordination Chemistry Reviews Volume 296, 15 July 2015, Pages 125-152
31 D. Aguila, P. Dechambenoit, M. Rouzieres, C. Mathoniere, R. Clerac, *Chem. Commun*., 2017, 53, 11588.
32 S. M. Nelson, P. D. A. Mcllroy, C. S. Stevenson, E. König, G. Ritter, J. Waigel, *J. Chem. Soc. Dalton Trans*., 1986, 991.
33 G. M. Sheldrick, *SHELX97. Program for the Refinement of Crystal Structures*, Univ. of Gottingen, Germany, 1997; G. M. Sheldrick, *Acta Crystallogr., Sect. A: Fundam. Crystallogr*., 2008, 64, 112.
34 A. Altomare, M.-C. Burla, M. Camalli, G. Cascarano, C. Giacovazzo, A. Guagliardi, A. G.-G. Moliterni, G. Polidori and R. Spagna, *J. Appl. Crystallogr*., 1999, 32, 115; L.-J. Farrugia, WinGX suite for small-molecule singlecrystal crystallography, *J. Appl. Crystallogr*., 1999, 32, 837.
35 E. Collet, P. Guionneau, *C. R. Chimie*, 2018, in press
36 a) T. Tayagaki, A. Galet, G. Molnar, M. Carmen Munoz, A. Zwick, K. Tanaka, J.-A. Real, A. Bousseksou, *J. Phys. Chem. B.*, 2005, 109, 14859; b) C. Enachescu, U. Oetliker, A. Hauser, *J. Phys. Chem. B.*, 2002, 106, 9540; c) R. Jakobi, H. Spiering, L. Wiehl, E. Gmelin, P. Gütlich, *Inorg. Chem*., 1988, 27, 1823; d) C. Enachescu, J. Linares, F. Varret, *J. Phys. Condens. Matter.*, 2001, 13, 2481; e) Z. Yu, T. Kuroda-Sowa, H. Kume, T. Okubo, M. Maekawa, M. Munakata, *Bull. Chem. Soc. Jpn.*, 2009, 82, 333; f) J.-D. Cafun, L. Londinière, E. Rivière, A. Bleuzen, *Inorg. Chim. Acta.*, 2008, 361, 3555.
37 a) C. Baldé, C. Desplanches, A. Wattiaux, P. Guionneau, P. Gütlich, J.-F. Létard, *Dalton Trans*., 2008, 2702; b) C. Baldé, C. Desplanches, M. Grunert, Y. Wei, P. Gütlich, J.-F. Létard, *Eur. J. Inorg. Chem*., 2008, 5382; c) C. Baldé, C. Desplanches, P. Gütlich, E. Freysz, J.-F. Létard, *Inorg. Chim. Acta.,* 2008, 361, 3529. d) C. Baldé, C. Desplanches, F. Le Gac, P. Guionneau, J.-F. Létard, *Dalton Trans.*, 2014, 43, 7820 ; e) C. Baldé, C. Desplanches, J-F. Létard,, G. Chastanet, *Polyhedron.*, 2017, 123, 138; f) G. Lebedev, S. Pillet, C. Baldé, P. Guionneau, C. Desplanches, J-F. Létard, *IOP Conf. Series: Materials Science and Engineering.*, 2009, 5, 012025 ; g) M-S. Sylla, C. Baldé, N. Daro, C. Desplanches, M. Marchivie, G. Chastanet, *Eur. J. Inorg. Chem*., 2017, 297-304; h) M-S. Sylla, C. Baldé, N. Daro, G. Chastanet, *J. Soc. Ouest-Afr. Chim*., 2017, 043, 37.
38 a) M. Sorai, J. Ensling, P. Gütlich, *Chem. Phys.*, 1976, 18, 199 ; b) P. Ganguli, P. Gütlich, E. W. Müller, *Inorg. Chem.*, 1982, 21 3429 ; c) J-P. Martin, J. Zarembovitch, A. Bousseksou, A. Dworkin, J.G. Haasnoot, F.Varret, *Inorg. Chem*., 1994, 33, 6325.
39 a) S. Zheng, M-A. Siegler, J-S. Costa, W-T. Fu, S. Bonnet, *Eur. J. Inorg. Chem.,* 2013, 1033–1042; b) R. Ohtani, S. Egawa, M. Nakaya, H. Ohmagari, M. Nakamura, L-F. Lindoy, S. Hayami, *Inorg. Chem*., 2016, 55, 3332−3337. c) P. Chakraborty, C. Enachescu, C. Walder, R. Bronisz, A. Hauser, *Inorg. Chem.*, 2012, 51, 9714; d) I. Krivokapic, P. Chakraborty, C. Enachescu, R. Bronisz, A. Hauser, *Inorg. Chem.*, 2011, 50, 1856 e) P. Chakraborty, R. Bronisz, C. Besnard, L. Guenée, P. Pattison, A. Hauser, *J. Am. Chem. Soc*., 2012, 134, 4049.
40 Mercury CSD 2.0 - New Features for the Visualization and Investigation of Crystal Structures, C. F. Macrae, I. J. Bruno, J. A. Chisholm, P. R. Edgington, P. McCabe, E. Pidcock, L. Rodriguez-Monge, R. Taylor, J. van de Streek and P. A. Wood, J. Appl. Cryst., 41, 466-470, 2008

Cite this: DOI: 10.1039/c0xx00000x

TOC Entry

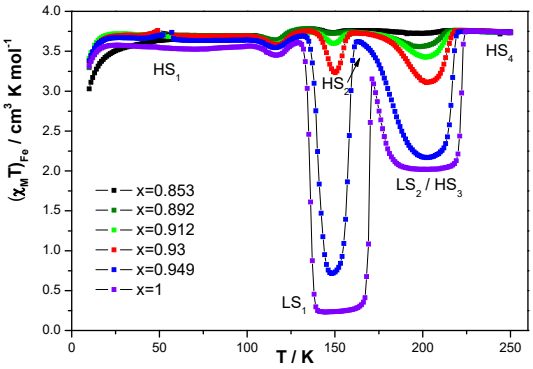

Temperature dependence of $(\chi_M T)_{Fe}$ for $[Fe_xMn_{1-x}(L_{222}N_3O_2)(CN)_2]\cdot H_2O$ of T(TIESST) experiment with x = 1 (in violet ■), 0.949 (in blue ■), 0.93 (in red ■), 0.912 (in green ■), 0.892 (in olive ■) and 0.853 (in black ■).